www.ietdl.org

Published in IET Generation, Transmission & Distribution
Received on 15th August 2011
Revised on 22nd February 2012
doi: 10.1049/iet-gtd.2011.0827

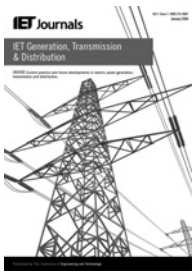

ISSN 1751-8687

Two-channel multirate network equivalent aimed to real-time electromagnetic transient calculation

G.D. Guidi Venerdini H.C. Zini G. Rattá

Instituto de Energía Eléctrica, Universidad Nacional de San Juan, Av. Libertador Gral. San Martín Oeste 1109 (J5400ARL), San Juan, Argentina
E-mail: gguidi@iee.unsj.edu.ar

Abstract: A computationally efficient multirate scheme was proposed to model a linear and time invariant part of an electric network for electromagnetic transient calculation. The main contribution is expected in the field of real-time calculation, where very efficient models are required to fulfil stringent time performance requirements. Two models of the equivalent sub-network based on different time steps are implemented in the low- and high-frequency channels of a basic Laplacian Pyramid unit. A detailed model based on the longest time step reproduces the low-frequency response, while a simplified (lower order) model, based on the shortest time step, reproduces the high-frequency behaviour. In this way, an accurate response of the equivalent over a wider frequency range can be achieved as compared with previous proposals based on a single low-frequency channel. Also, the proposed scheme make a much greater flexibility in choosing the decimation factor possible as compared with a previous proposal of two co-authors based on a 2-fold decimated filter banks.

1 Introduction

Real-time digital simulation of electromagnetic transients is possible relatively recently through the digital transient network analysers (DTNA). This equipment is used in the development or setting of devices such as protection relays or control systems for power electronics, by connecting them to network models through interfaces that allow closed loop simulations.

Despite the high-calculation speed of modern digital processors, real-time simulation of electromagnetic transients is still a challenging task [1–6], mainly when the network model include high-speed electronic switches or when protective relays based on or affected by the high-frequency network response have to be tested [7–11]. In this context, the development of highly sophisticated models, able to reproduce a wide band spectrum of the network response with minimum computational requirement is important [12–16]. In this sense an interesting approach is the use of multirate schemes, where, roughly speaking, a linear and time invariant part of the network not directly involved in the simulated switching (from now on the equivalent sub-network) is modelled using a larger time step. In previously proposed multirate schemes [17–20], the equivalent sub-network model is implemented in a single (low frequency) channel as shown in the block diagram of Fig. 1. There, the downsampler $[\downarrow M]$ indicates that only one each M value available at its input is processed by the block connected to its output. The low-pass, linear phase, anti-aliasing filter $H(z)$ attenuates the components with frequencies $|\omega| > \pi/(M\Delta t)$ rad/s at the output of the main sub-network model to prevent their alias to appear in the input of the equivalent model. Restoring the original time step at the output of the equivalent sub-network, can be seen as a two stage process: first the up-sampler $[\uparrow M]$ interleaves $M-1$ null values between successive inputs (which amount to replicates $M-1$ times the spectrum of the signal), then the null samples are replaced by interpolated values computed by the interpolation filter $G(z)$ (a process that attenuate the $M-1$ replicas or images).

It is clear that, apart from the filters, the computational cost of the equivalent is reduced to the same extent the decimation factor M is increased but, as it is apparent too, the bandwidth of the model is narrowed alike; in other words, the decimation factor M is essentially limited by the required bandwidth of the equivalent sub-network model.

The key idea behind the proposed modelling scheme is that model accuracy (specifically its bandwidth) can be substantially improved for the same computational requirements by including a second channel to model the high-frequency response. The model in this channel runs with the same time step as the main sub-network model. It is clear that in order for this to be possible a larger time step has to be used in the low-frequency channel and a very simple model in the high-frequency one. A previous paper of two co-authors first develops this idea but for an equivalent model based on two 2-fold decimated channels [21]. The scheme proposed here allows higher-decimation factor in the low-frequency channel as well as more flexibility in the design of the filters. The potential application of the proposed model is in the field of real-time simulation of electromagnetic transients, mainly in cases where a wide model bandwidth is required such as in the development and setting of transient-based protection of transmission lines, or power electronic devices with high-speed electronic switches.

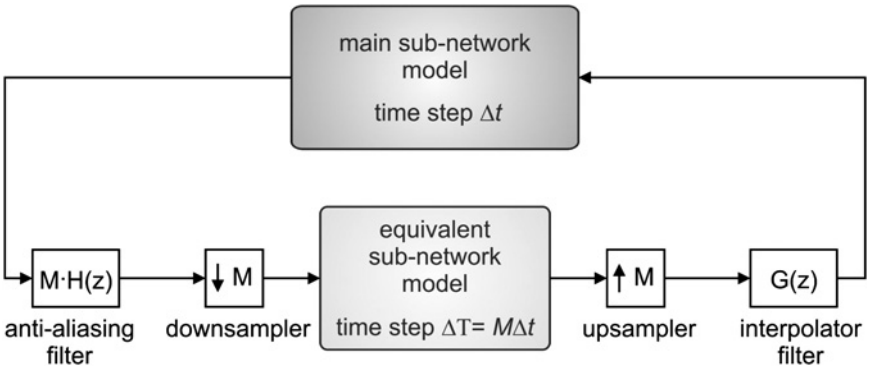

Fig. 1 *Basic single channel multirate system*

The study organisation is as follow: Section 2 describes the structure of the proposed multirate equivalent. Frequency domain analysis is applied in Section 3 to explain how it works. In Section 4 a specific structure is proposed for the low- and high-frequency models as well as the procedure to obtain their parameters. In Section 5 the proposal is validated with a test case. Finally, conclusions are presented in Section 6.

2 Structure of the multirate equivalent

Fig. 2 shows the structure of the proposed two-channel model; the low- and high-frequency models of the equivalent sub-network ($F_{\mathrm{LF}}(z)$ and $F_{\mathrm{HF}}(z)$) are located in the corresponding channels of a basic Laplacian pyramid unit [22]. Transfer functions $H(z)$ and $G(z)$ are again low-pass unity gain linear phase filters with cut-off frequency below $\omega_N = \pi/(M\Delta t)$ rad/s designed to avoid aliasing and imaging. Thus, the part of the block diagram enclosed in the dashed rectangle works the same way as the single decimated channel model shown in Fig. 1.

Before analysing the complete scheme it would be useful to observe that when $F_{\mathrm{LF}}(z)$ and $F_{\mathrm{HF}}(z)$ are unit gains, the output y would simply be a delayed version of the input, since it is obtained by first subtracting and then adding the same signal (x'_{LF}) to the output of the D samples delay z^{-D}. By analysing the frequency contents of the signals in the complete scheme the following can be observed: The nature of $H(z)$ makes x' a delayed low-frequency approximation of the input signal with negligible amplitude in the rejection band, let's say above ω_c, been ω_c the frequency cut of the filter $H(z)$. Making $\omega_c < \pi/(M\Delta t)$, the down-sampled signal x_{LF} (input of the low-frequency model F_{LF}) is free from aliasing, and its spectrum, that spans the interval $|\omega| < \pi/(M\Delta t)$ rad/s, contains the non negligible part of $X'(e^{j\omega\Delta t})$, that is the low-frequency components of the input. Furthermore, x_{LF} and its up-sampled version have the same spectrum in the interval $|\omega| < \pi/(M\Delta t)$ rad/s, which is periodically extended in the last one, until covering the band $\pi/(M\Delta t) < |\omega| < \pi/\Delta t$ rad/s. These periodic replicas are filtered by the linear phase low-pass filter $G(z)$, keeping the low-frequency content almost unchanged in x'_{LF} except for an extra delay. It is now clear that if the delay D is equal to the whole group delay of $H(z)G(z)$, the low-frequency components of $x(n-D)$ and $x'_{\mathrm{LF}}(n)$ will be in phase and (approximately) cancel each other when subtracted. Hence, x_{HF} (to be processed by the high-frequency model) is a delayed approximation of the high-frequency spectrum of the input signal as required.

The D samples' delay is a constraint to the nature of the input–output relationships the proposed equivalent can model. In effect, since driving point impedances or admittances do not have such delays, the described multirate scheme is unsuitable to implement classic Thevenin or Norton equivalents. An interesting possibility first applied in [20] and also in [21], is to use the delay to model part of the travelling time of a line connecting the main and the

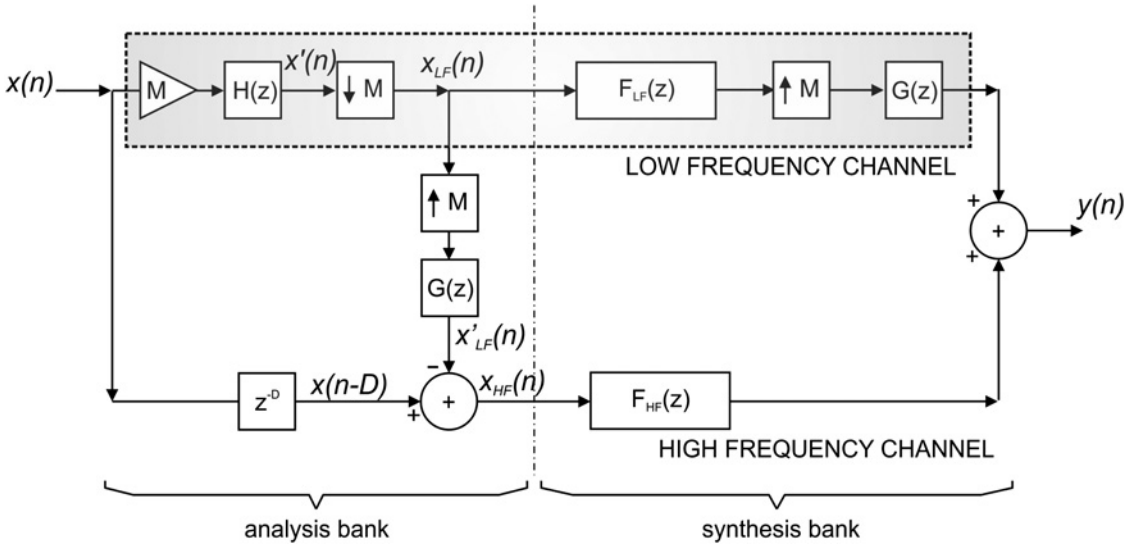

Fig. 2 *Structure of the proposed equivalent model*

equivalent sub-networks. The basic arrangement is shown in Fig. 3. The device to be tested in a real-time implementation of Fig. 3*b* is connected to sub-network A while B is represented by the equivalent. A line, here assumed lossless and with an integer travel time $\tau = n\Delta t$, connects them.

Waves travelling along this line are the interface of both models: J_i and K_i are the incident and reflected current waves at line end I; the analysis bank decomposes J_b into its low- and high-frequency components with time steps $M\Delta t$ and Δt, respectively, which are the inputs of the low- and high-frequency models. Conversely, the synthesis bank combines the two components K_{bLF} and K_{bHF} into the full band signal K_b. Line-end models relate the incident wave and the line voltage (inputs) to the reflected wave and the line current (outputs). The delay the filters of the analysis and synthesis banks introduce is compensated by reducing the delay that explicitly models the travelling times; notice that though $D/2$ samples have been embedded in each explicit delay $z^{-(n-D/2)}$, any other partition of D is possible since it does not affect the input to the main sub-network model (e.g. $z^{-(n-(D+1)/2)}$ and $z^{-(n-(D-1)/2)}$ if D is odd). A distributed parameter transmission line model is described in greater detail later.

3 Frequency domain analysis

The input–output relationship of the multirate scheme of Fig. 2 can be written in the frequency domain as

$$\begin{aligned} Y(e^{j\omega\Delta t}) = e^{-jD\omega\Delta t}[&F_{LF}(e^{j\omega M\Delta t})P(e^{j\omega\Delta t}) \\ &+ F_{HF}(e^{j\omega\Delta t})(1 - P(e^{j\omega\Delta t}))]X(e^{j\omega\Delta t}) \\ &+ [F_{LF}(e^{j\omega M\Delta t}) - F_{HF}(e^{j\omega\Delta t})]G(e^{j\omega\Delta t})\tilde{X}_{LF}(e^{j\omega\Delta t}) \end{aligned} \quad (1)$$

where

$$P(e^{j\omega\Delta t}) = e^{jD\omega\Delta t}H(e^{j\omega\Delta t})G(e^{j\omega\Delta t}) \quad (2)$$

$$\tilde{X}_{LF}(e^{j\omega\Delta t}) = \sum_{k=1}^{M-1} H(e^{j(\omega\Delta t - 2k\pi/M)})X(e^{j(\omega\Delta t - 2k\pi/M)}) \quad (3)$$

The signal $\tilde{X}_{LF}$ in the second term of (1) is obtained by adding $M-1$ shifted images of $X' = H(z)\cdot X$ (3), in such a way that the low-frequency content ($|\omega| < \pi/(M\Delta t)$) of x' is moved to the high part of the spectrum of $\tilde{x}_{LF}$ and conversely.

As a consequence, the response of the second term of (1) to a sine wave is a set of $M-1$ sinusoid of different frequency. This is clearly an aliasing/imaging error of the model that should be made suitably small by a proper selection of the filters. In effect, $G(z)$ in (1) attenuate the high frequencies of the alias, originated in the low frequencies of the X [not attenuated by $H(z)$ in (3)], and conversely $H(z)$ in (3) attenuate the high frequencies of X which alias are in the low frequencies of Y [i.e. non-attenuated by $G(z)$ in (1)].

However, the first term of (1) is the part of the response free from aliasing; $F_{LF}(e^{j\omega\Delta t})$ is merely the periodic extension over the interval $|\omega| < \pi/\Delta t$ of the response of the low-frequency model $F_{LF}(z)$, which is defined on the interval $|\omega| < \pi/(M\Delta t)$. Beside, according to (2), $P(z)$ is a unity gain, delay free, low-pass filter with frequency response $P(e^{j\omega\Delta t}) = |H(e^{j\omega\Delta t})||G(e^{j\omega\Delta t})|$, and $1 - P(z)$ is its high-pass complement.

Fig. 4 illustrates the relationship between these frequency responses in the first term of (1) for $M = 4$.

It can be see that in the pass-band of $P(z)$, the response is dictated by $F_{LF}(e^{j\omega M\Delta t})$ and specifically by the low-frequency model because the pass-band of $P(z)$ does not extend beyond its first period; conversely, in the rejection band of $P(z)$, the response is determined by high-frequency model $F_{HF}(e^{j\omega M\Delta t})$. A smooth transition from one to the other takes place in the transition band.

4 Proposed structure and procedure for obtaining the low- and high-frequency models

The previous sections describe the configuration of the proposed multirate equivalent from which different implementation are possible according to the choices made regarding the structure of the low- and high-frequency models $F_{LF}(z)$ and $F_{HF}(z)$. In this section a quite natural implementation with models based on the electromagnetic transients program (EMTP) [25] formulation is outlined, together with the procedure applied to calculate their parameters.

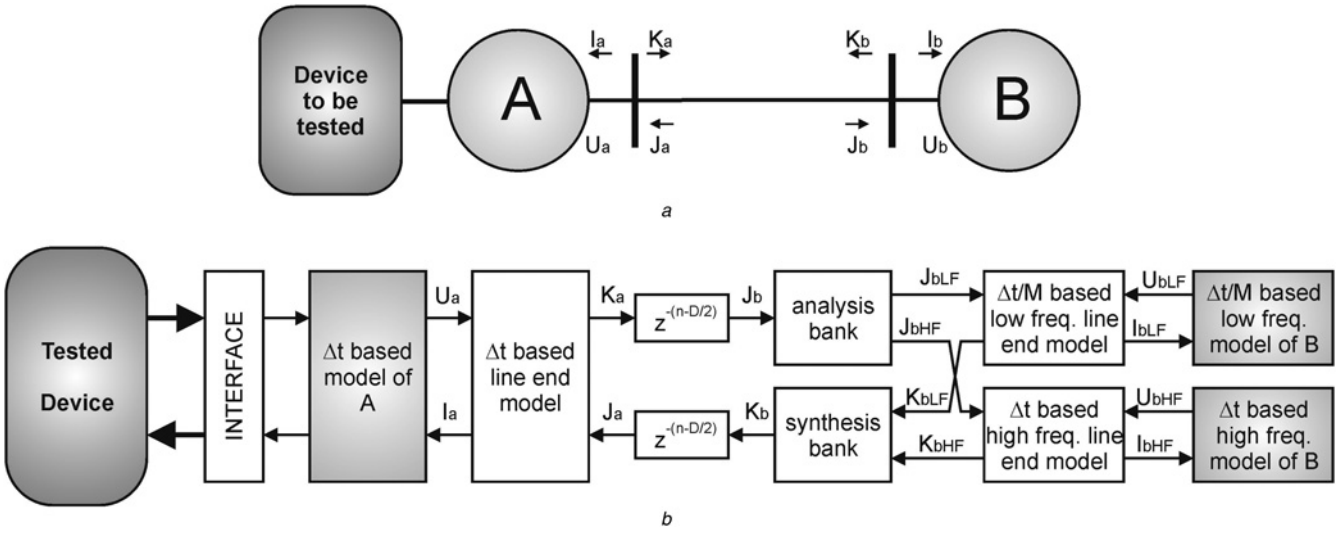

Fig. 3 *Basic arrangement of the proposed multirate system*

a Main (A) and equivalent (B) sub-networks connected through the interface line
b Block diagram of the multirate scheme of *a*

doi: 10.1049/iet-gtd.2011.0827

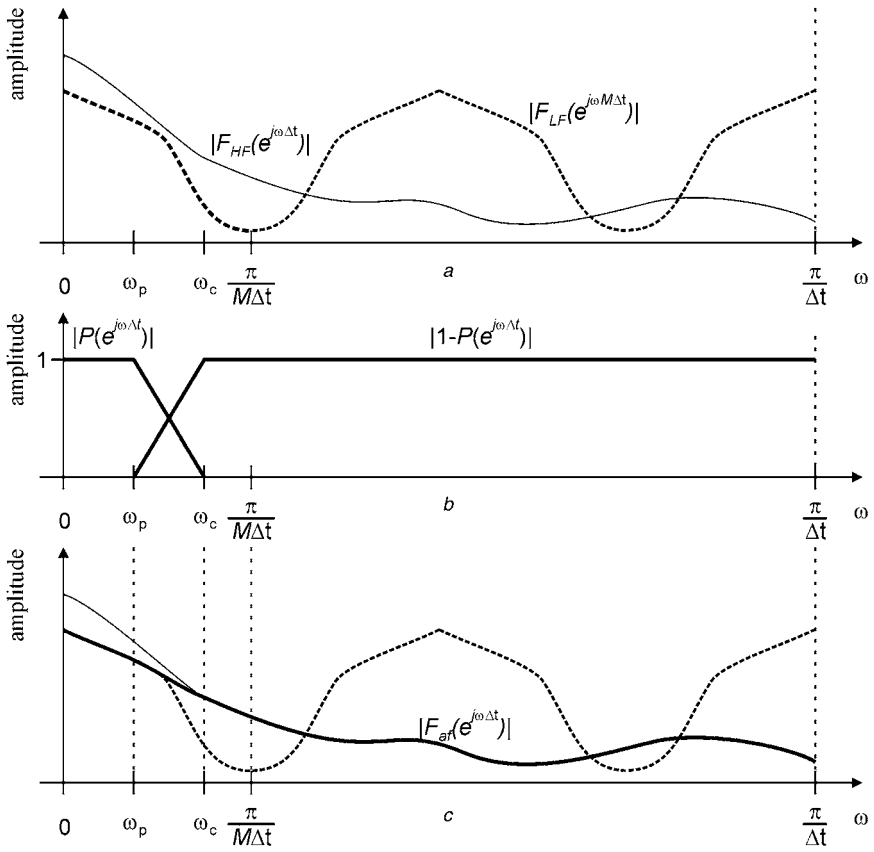

Fig. 4 *Illustrative examples of*

a Frequency response of the amplitude of low- and high-frequency models ($F_{\mathrm{LF}}(z)$ and $F_{\mathrm{HF}}(z)$)
b Frequency response of the amplitude of filters $P(z) = z^{D}H(z)G(z)$ and $1 - P(z)$
c Composition of the amplitude of $F_{\mathrm{LF}}(z)$ and $F_{\mathrm{HF}}(z)$ to form $F_{\mathrm{af}}(z)$, the aliasing free part of the equivalent model

4.1 Structure of the low- and high-frequency models

Classic representations of a sub-network comprise transmission lines and circuits of resistive inductive and capacitive (RLC) components that model the substations. In both $F_{\mathrm{LF}}(z)$ and $F_{\mathrm{HF}}(z)$, lines are represented using a scheme based on the JMarti model of EMTP [26], and substations models are obtained by discretising the differential equations of inductances and capacitors through the trapezoidal rule.

Fig. 5 shows the block diagram of the line model and the way it connects to a substation one. For the sake of simplicity only one line-end is represented in detail. Notice that the same scheme applies to the low- and high-frequency channel, though with different time steps and transfer function orders.

The single phase scheme shown refers to any (positive, negative or zero) sequence. Incident and reflected current waves (J and K, respectively) are positive when flow in the same direction they travel. $\mathrm{Zc}(z)$ and $A(z)$ are discrete transfer functions that, respectively, model the characteristic impedance and the distortion the waves experience when travel the entire line length; that is they approximate

$$\mathrm{Zc}(\omega) = \sqrt{\frac{R' + j\omega L'}{G' + j\omega C'}} \tag{4}$$

and

$$A(\omega) = \mathrm{e}^{j\omega\tau}\mathrm{e}^{-jl\sqrt{(R'+j\omega L')(G'+j\omega C')}} \tag{5}$$

where l is the line length and R', L', G' and C' are transmission line parameters per unit length. Delays z^{-n} represent the integer part of the travelling time $\tau = (n + a)\Delta t$, while the fractional part ($a\Delta t$) is included in $A(z)$. The factor a represents the part of the travel time that cannot be represented by a step time, because it is inferior than one Δt (in fact, $0 < a < 1$). When a is not 0, then a linear interpolation could be done to obtain an approximation of the incident wave J. For example, the incident wave J_{a2} of Fig. 5*b* is calculated by $J_{a2}(z) = z^{-n}((1 - a) + az^{-1})A(z)K_{a1}(z)$. So, the factor $((1 - a) + az^{-1})$ could be included in $A(z)$, doing $A'(z) = ((1 - a) + az^{-1})A(z)$ and replacing $A(z)$ by $A'(z)$ in the scheme of Fig. 5*b*.

Discrete state space (6) are obtained by properly combining the substation and associated line-ends models

$$\begin{aligned} \boldsymbol{X}(i+1) &= [\mathrm{A}]\boldsymbol{X}(i) + [\mathrm{B}]\boldsymbol{J}(i) \\ \boldsymbol{K}'(i) &= [\mathrm{C}]\boldsymbol{X}(i) + [\mathrm{D}]\boldsymbol{J}(i) \end{aligned} \tag{6}$$

with $\boldsymbol{X}$: vector of states or history terms and $\boldsymbol{J}$ and $\boldsymbol{K}'$: vectors of incident and reflected current waves.

Each integration step of the corresponding channel, (6) of each substation is used to update variables K' in terms of the inputs J (already computed as outputs of the opposite line-ends) and the states X.

Clearly this scheme reproduces one of the most outstanding characteristic of EMTP, that is decoupling of equations of different substations and associated line-ends, which allows a very natural parallelisation scheme: decoupled equations

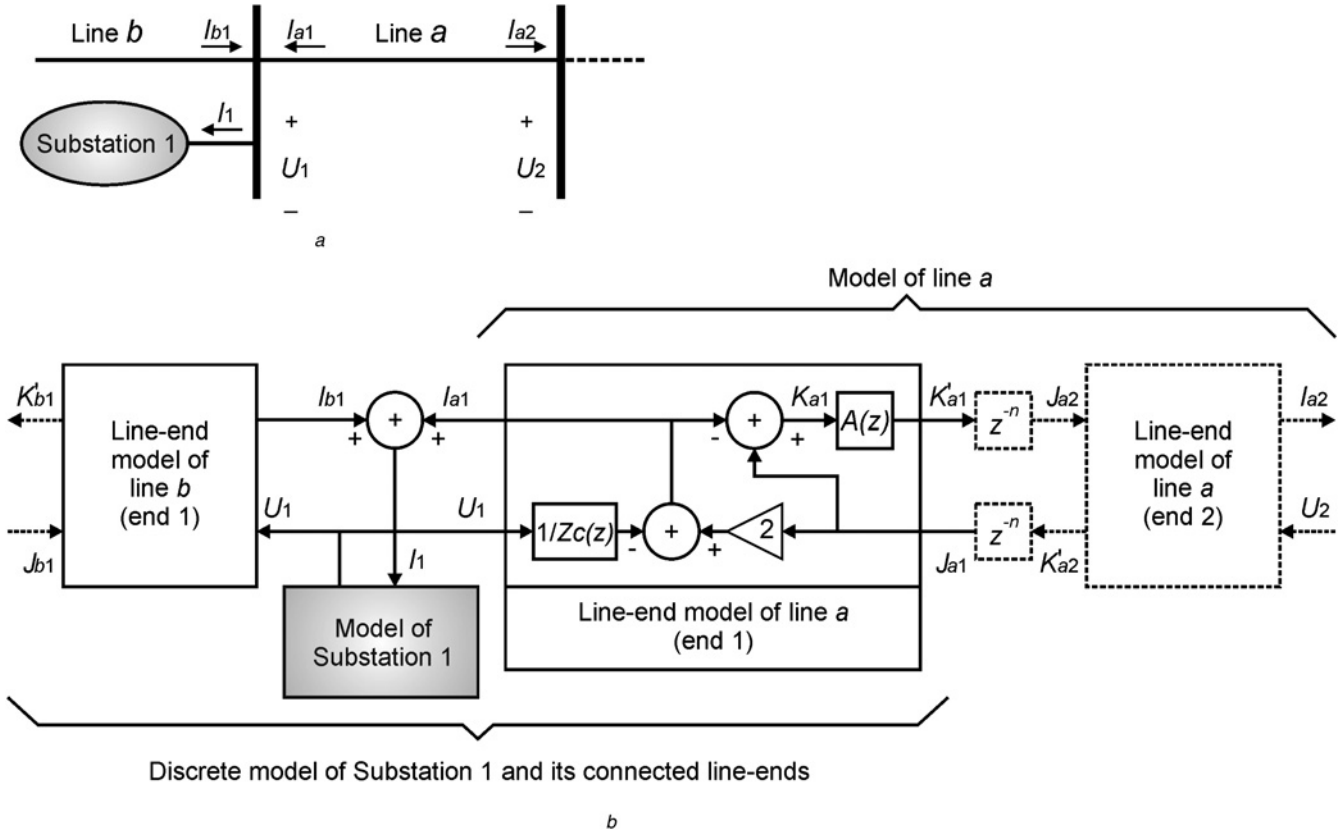

Fig. 5 *Single phase line model of the JMarti type and its connection to a substation model*

a Substation and connected lines
b Block diagram of the model of *a*

sets can be solved in different processors that only communicate previously computed values.

Total number of basic math operation for an optimal realisation of the discrete model of a substation with m connected lines is $Np = 2(n_{LC} + \mathrm{n}_{AZ})m + m^2$ products and $Na = Np - m + 1$ sums, where n_{LC} is the number of inductances and capacitors in the substation model (trapezoidal rule assumed) and n_{AZ} is the total order of the connected lines $A(z)$ and Zc(z) transfer functions.

4.2 Parameters calculation outline

4.2.1 Line functions: Routine Line Constant and the JMarti setup of EMTP provide poles and residues of continuous transfer functions Zc(s) and $A(s)$ that fit (4) and (5) over a wide bandwidth. Then, discrete transfer functions $A(z)$ for the low- and high-frequency models are obtained from $A(s)$ through model order reduction and discretisation using a Steiglitz–McBride iteration algorithm (stmcb function in Matlab). This algorithm iteratively adjusts the coefficients of a rational function $A(z)$ of user specified order so as to minimise the squared error of its time domain response to a given input signal. The spectrum of the input signal used is mainly concentrated in the band covered by the channel the transfer function is intended for. The same procedure is applied to obtain the low-frequency approximation of the characteristic impedance (Zc(z)), while a constant value is used in the high frequencies instead of a function.

Along the research we found that for typical EHV overhead transmission lines, decimation factor M around 10, and irrespective of the sequence, an adequate balance of accuracy and computational requirements of the resulting models is usually reached with transfer functions $A(z)$ and Zc(z) of order 4 and 7, respectively, in the low-frequency channel, and $A(z)$ of order 1 in high-frequency. As an example Fig. 6 compares the frequency response of $A(z)$ and Zc(z) with the indicated orders with $A(s)$ and Zc(s) (JMarti fitting), for the positive sequence of 240 km, 500 kV overhead transmission line. These transfer functions are part of the model of Section 5 where transition band of $P(z)$ spans de interval (2 kHz, 4.5 kHz), and the time steps of $F_{\mathrm{HF}}(z)$ and $F_{\mathrm{LF}}(z)$ are 10 and 100 μs ($M = 10$).

4.2.2 Substation model: In order to reduce the order of $F_{\mathrm{HF}}(z)$, also substation models can usually be simplified as previously proposed in [21].

In effect, the only way RLC circuits interact with the rest of the network is through the travelling waves, which behaviour is determined by the reflection and transmission coefficients. Denoting Y the driving point admittance of the substation, and Yc_i, $i = 1, \ldots, m$ the characteristic admittances of the connected lines, the reflection and transmission coefficients, respectively, are

$$\frac{K_i}{J_i} = \frac{2Yc_i - \left(Y + \sum Yc_k\right)}{Y + \sum Yc_k} \quad \text{and} \quad \frac{K_j}{J_i} = \frac{2Yc_j}{Y + \sum Yc_k}$$

In addition, circuits modelling typical substations usually are RL branches, or behave like them at high frequencies; therefore, above a certain frequency it is $Y \ll \sum Yc_k$ and the entire circuit can be disregarded with no significant change in the model response. For circuit modelling typical substation and reasonable decimation factors (e.g. $M = 10$),

doi: 10.1049/iet-gtd.2011.0827

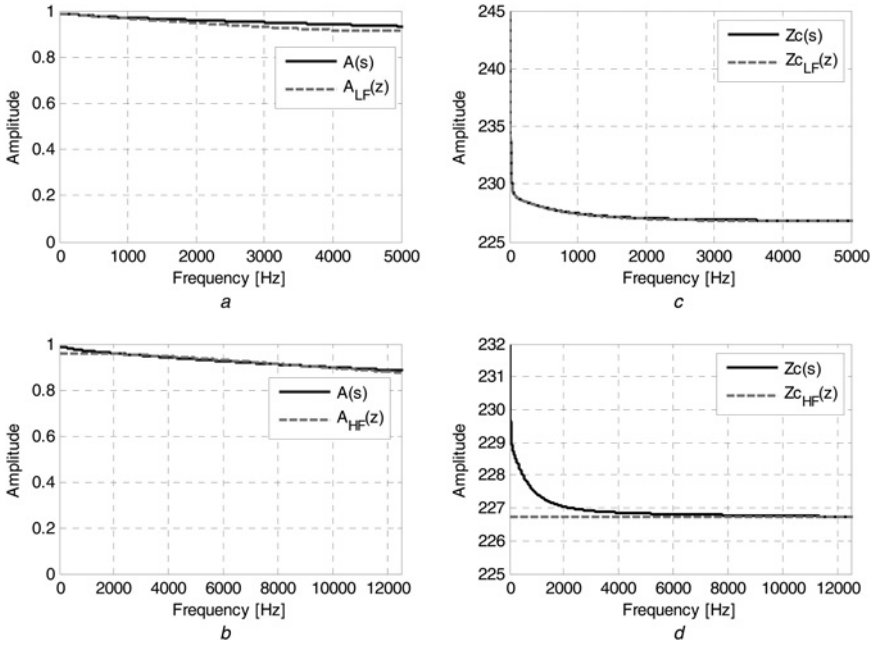

Fig. 6 *Low- and high-frequency fitting of line functions Zc(ω) and A(ω)*

a Low-frequency fitting of $A(\omega)$
b High-frequency fitting of $A(\omega)$
c Low-frequency fitting of $Zc(\omega)$
d High-frequency fitting of $Zc(\omega)$

this simplification is very often valid at the frequencies the high-frequency model is devoted to. This is the case for all the substations in the example of Section 5.

4.2.3 Filters specification: Anti-aliasing and anti-imaging filters $H(z)$ and $G(z)$ are linear phase with cut-off frequencies lower than $\pi/\Delta t$ to avoid aliasing.

As it is the common practice, anti-imaging filters $G(z)$ are interpolators, that is, ones that fill the zero samples of the upsampler output, keeping unchanged those non-nulls. Specification of interpolator includes the upsampling factor (M) and the number of non-zero samples used for interpolation.

Complete filter specification of $H(z)$ include the maximum allowable ripple in the pass band, the minimum required attenuation in the stop band and the lower and upper edges of the transition band ω_p and ω_c. Whereas only a little dose of judgement is required to define the first two items, proper selection of band edges is not clearly apparent.

Suitable ω_p and ω_c can however be obtained by solving a simple optimisation problem to minimise the error of the aliasing free term of (1) for the obtained low- and high-frequency models, the selected interpolator G, and an idealised filter H with linear variation in the transition band; that is

$$\begin{cases} \min\limits_{\omega_p,\omega_c} \|F(e^{j\omega\Delta t}) - [F_{\mathrm{LF}}(e^{j\omega M\Delta t})|G(e^{j\omega\Delta t})||H_{id}(\omega_p, \omega_c, \omega)| \\ \qquad + F_{\mathrm{HF}}(e^{j\omega\Delta t})(1 - |G(e^{j\omega\Delta t})||H_{id}(\omega_p, \omega_c, \omega)|)]\| \\ \omega_c < \dfrac{\pi}{M\Delta t} \end{cases}$$

with $F(e^{j\omega\Delta t})$ the desired frequency response of the multirate

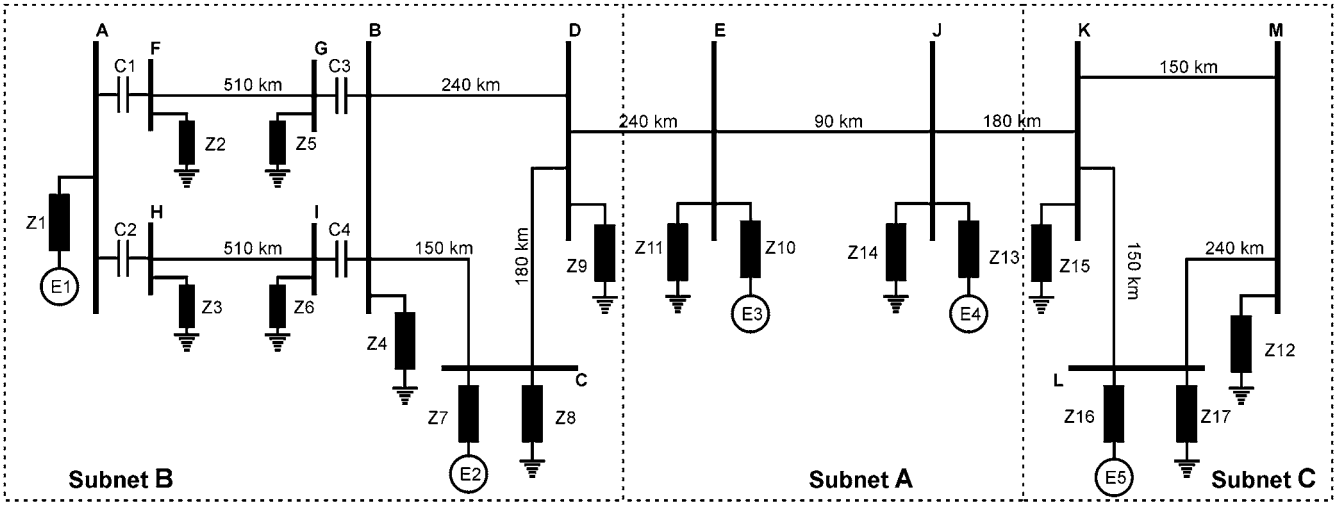

Fig. 7 *Single-line diagram of the network used for model validation*

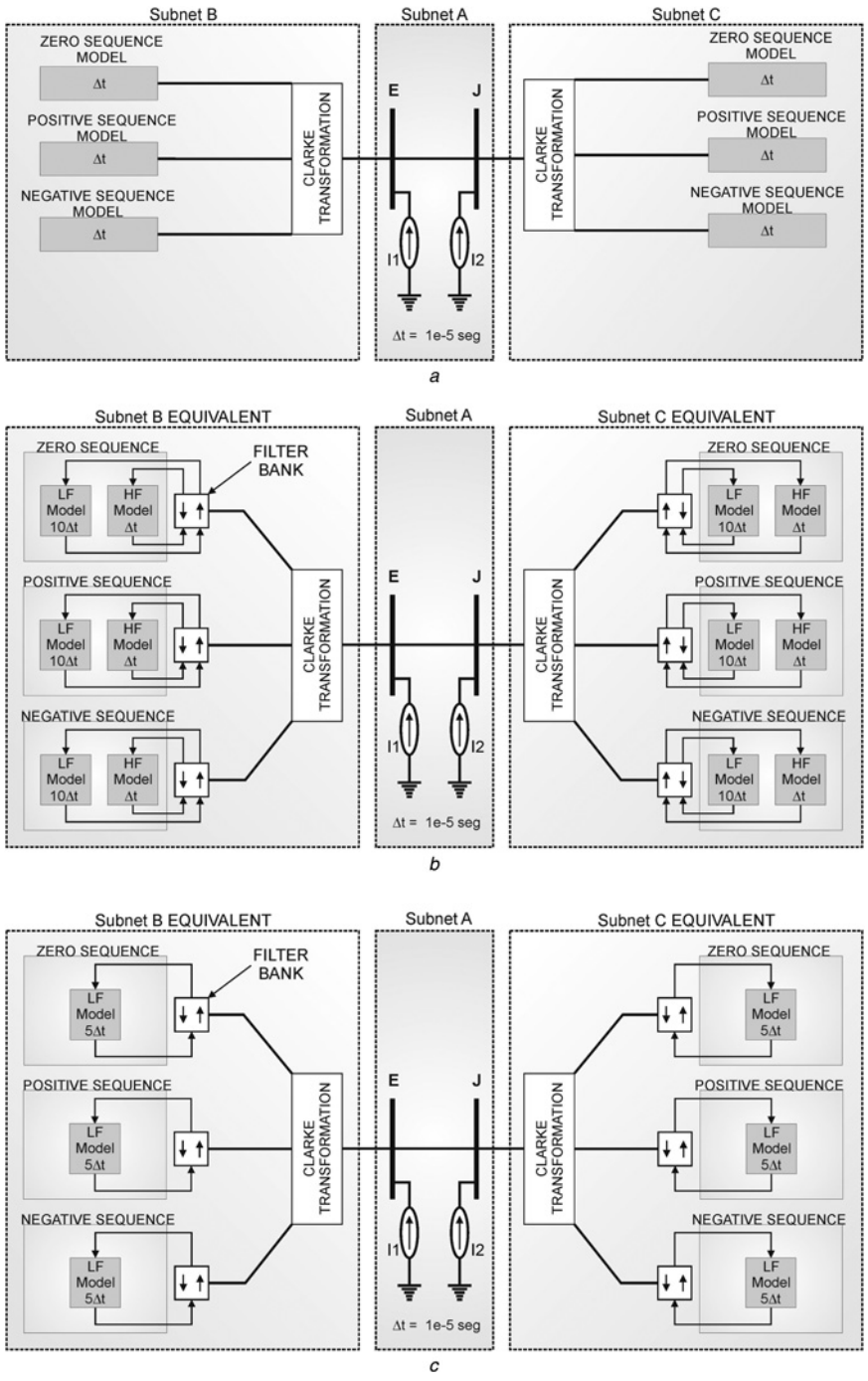

Fig. 8 *Diagram of*

a Conventional model (MC)
b Two-channel multirate model (MMD)
c Single-channel multirate model (MM1C)

Table 1 Products performed each time step of A by subnets B and C

	MC	MMD	MM1C
low-frequency model	3558	3558/10 = 355.8	3558/5 = 711.6
high-frequency model	–	414	–
subtotal	3558	355.8 + 414 = 769.8	711.6
filters	–	93	151.2
total products	3558	769.8 + 93 = 862.8	711.6 + 151.2 = 862.8
save achieved respect the conventional scheme	–	75.75%	75.75%

doi: 10.1049/iet-gtd.2011.0827

Table 2 Additions performed each time step of A by subnets B and C

	MC	MMD	MM1C
low-frequency model	3525	3525/10 = 352.5	3525/5 = 705
high-frequency model	–	381	–
subtotal	3525	352.5 + 381 = 733.5	705
filters	–	91.2	148.8
total additions	3525	733.5 + 91.2 = 824.7	705 + 148.8 = 853.8
save achieved respect the conventional scheme	–	76.60%	75.78%

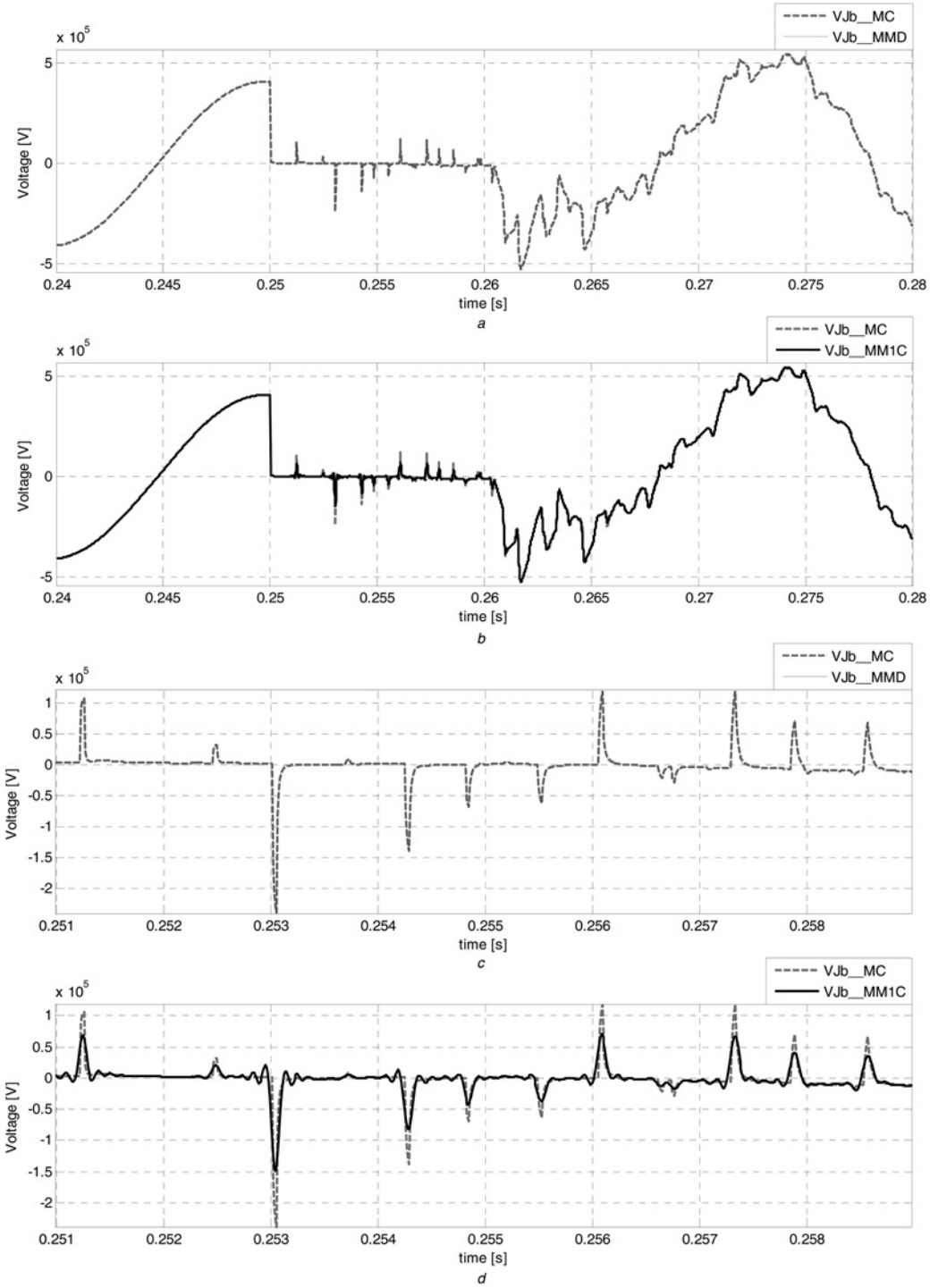

Fig. 9 *Two phases to ground fault – bus J voltage at a faulted phase*

a Comparison of schemes MC and MMD
b Comparison of schemes MC and MM1C
c Zoom to *a*
d Zoom to *b*

equivalent, and

$$|H_{id}| = \begin{cases} 1 & \omega < \omega_p \\ (\omega - \omega_c)/(\omega_p - \omega_c) & \omega_p \le \omega \le \omega_c \\ 0 & \omega > \omega_c \end{cases}$$

Additional constraints can be included regarding the transition band width $(\omega_c - \omega_p)$ in order to limit the filter order needed to achieve the required ripple and attenuation.

In the practice we found that filters $H(z)$ and $G(z)$ which orders add up $\sim$120 are required. Computational cost of so large filters, can however be substantially reduced because (upsampling and downsampling) only one each M input of G is non-zero, and $M-1$ each M outputs of H are disregarded. Optimal implementations that take advantage of this fact, known as poly-phase decimation and interpolation [23], allow reducing the computational cost by a factor $1/M$ as compared with standard implementations.

5 Model validation

The network shown in Fig. 7 is used to demonstrate the accuracy of the proposed multirate scheme. To this purpose three models have been implemented in the Matlab/Simulink [24] platform

- *Conventional model (MC):* The whole network is modelled based on time step $\Delta t = 1e-5$ s.
- *Developed multirate model (MMD):* Sub-network A is modelled as in MC and sub-networks B and C through the proposed multirate scheme with a decimation factor $M = 10$.
- *Multirate one channel model (MM1C):* Sub-network A is modelled as in MC and sub-network B and C through a single channel multirate equivalents with a decimation factor $M = 5$.

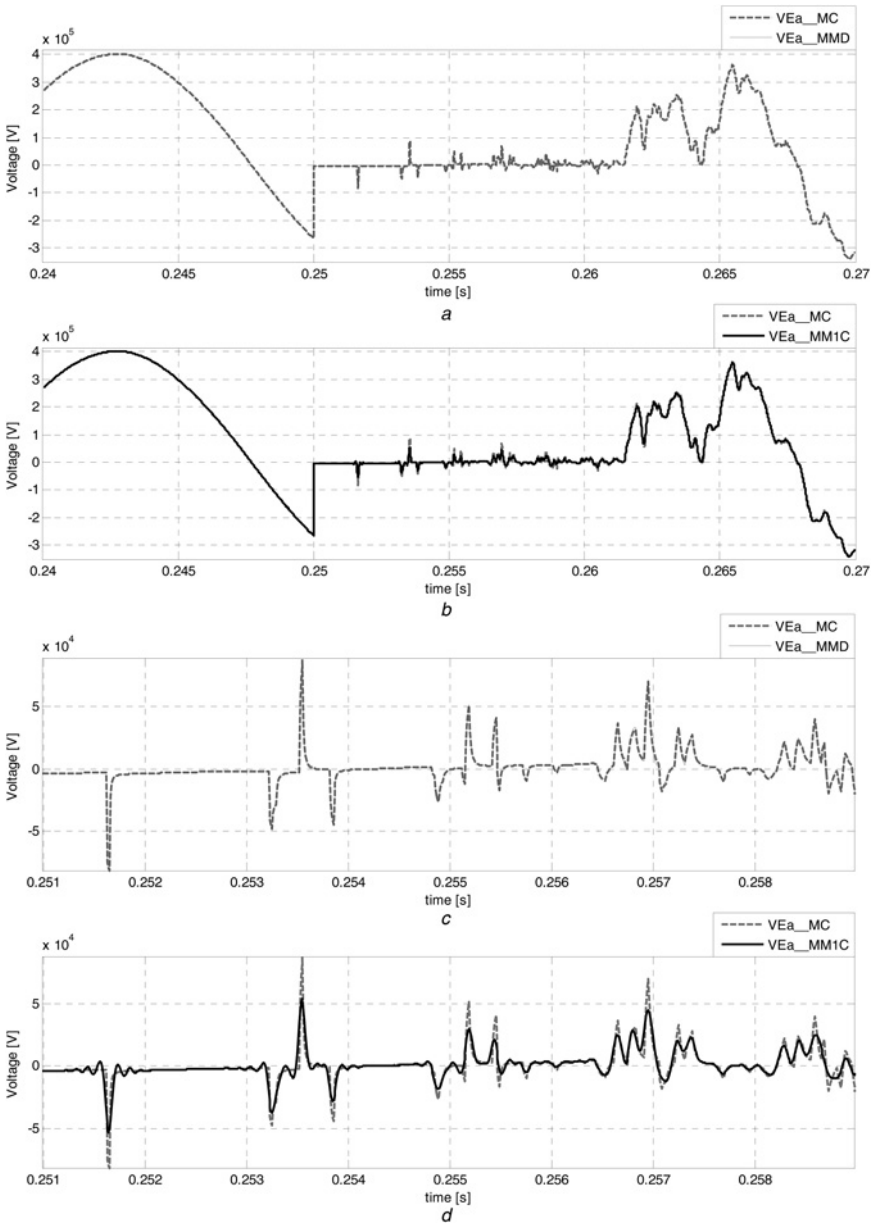

Fig. 10 *Three phase to ground fault – bus E voltage, phase A*

a Comparison of schemes MC and MMD
b Comparison of schemes MC and MM1C
c Zoom to *a*
d Zoom to *b*

doi: 10.1049/iet-gtd.2011.0827

Decimation factor of MM1C has been chosen so that both multirate equivalents perform almost the same number of math operation per unit of simulated time.

Substation and line models have been obtained with the procedure outlined in Section 4. Filters $H(z)$ and $G(z)$ of order 76 and 38 in MMD and 76 and 48 in MMC1 have been implemented.

5.1 Network model

The test network comprises nine buses and 11 transmission lines. The model is three-phase. Frequency-dependent transmission line models of the JMarti type outlined in Section 4.1 have been used for all the lines, with transfer functions $A(z)$ of order 4 and Zc(z) of order 7, except in high-frequency model of MMD where orders, respectively, were 1 and 0 (i.e. constant). The main parameters of the test system and its implemented models are shown in the Appendix.

Fig. 8 shows the block diagrams of the modelled schemes with the integration steps used. Sources connected to buses E and J are Norton current sources taking into account all the power frequency sources in the network.

5.2 Computational requirements of the modelled schemes

Tables 1 and 2 summarise the number of products and additions performed by the models of sub-networks B and C each integration step of sub-network A. Math operations concerning sub-network A and Clarke transforms are not included as they are the same in the three schemes. It should be noted that the computational savings in both multirate schemes is 75% with respect to the conventional one (Tables 1 and 2).

6 Results

Two simulated manoeuvers are shown in the plots of Figs. 9 and 10: A two-phase to ground and a three-phase to ground fault of line EJ, near bus J and E, respectively, both followed by three-phase fault clearing. Times of fault inception and clearing are $t_f = 0.25$ s and $t_{op} = 0.26$ s in both cases (effective opening at zero crossing of circuit breaker currents). Unrealistically fast fault clearing have been considered in order to reduce the number of plots necessary to cover the relevant aspects of the transients with enough details.

The following remarks may be in order: As it is expected, both multirate models (MMD and MM1C) are very accurate at low frequencies (begin and end of plots in Figs. 9*a*, *b*, 10*a* and *b*). Both models are also very accurate in the medium-frequency range prevailing some milliseconds after fault clearing. This good performance is achieved through different mechanism however, using a relatively short-time step (50 μs) in the single channel equivalent, and through the contribution of the high-frequency model in the medium-frequency range in the two-channel equivalent. Finally Figs. 9*c* and 10*c* show an excellent agreement between the proposed equivalent and the full model at high frequencies, in contrast with plots in Figs. 9*d* and 10*d* where the excessive attenuation makes apparent a poor modelling in the high-frequency range.

7 Conclusions

A novel two channels multirate equivalent to model linear and time invariant part of power systems in electromagnetic transient simulation has been developed. As in previous proposals based on a single decimated channel, a low-frequency model of the equivalent sub-network is implemented using a larger time step than the one used for the main sub-network. The developed scheme, however, includes an additional, non-decimated channel, where a very simple model is implemented to take into account the high-frequency response. Sub-network models are implemented in the channels of a basic Laplacian Pyramid unit. This well-known multirate scheme allows (almost conceptually) arbitrary integer decimation factors and very flexible selection of the filters; thus overcoming the main drawback of a previous proposal of two co-authors based on 2-fold decimated filter banks. A structure based on the EMTP formulation is proposed for the low- and high-frequency sub-network models, and the procedure for obtaining the corresponding model parameters has been outlined.

Theoretic analysis and results of the reported test case show that a wider model bandwidth can be achieved with the developed scheme without increasing the computational requirements. In the authors opinion the proposed two channels multirate equivalent could be a valuable contribution in the field of real-time simulation of electromagnetic transients, mainly in cases where a wide model bandwidth is required such as in the development and setting of transient-based protection of transmission lines, or power electronic devices with high-speed electronic switches.

It has to be noticed that the proposed model can be modelled only linear elements. It is important to apply the model only to those parts of the network that are not directly affected by the transient under study, ensuring that those parts never reach saturation levels. However, nonlinear elements can be modelled outside the equivalent, in the main part of the network to be modelled.

8 References

1 Chen, Y., Dinavahi, V.: 'FPGA-based real-time EMTP', *IEEE Trans. Power Deliv.*, 2009, **24**, (2), pp. 892–902

2 Nie, X., Chen, Y., Dinavahi, V.: 'Real-time transient simulation based on a robust two-layer network equivalent', *IEEE Trans. Power Deliv.*, 2007, **22**, (4), pp. 1771–1781

3 Chen, Y., Dinavahi, V.: 'Digital hardware emulation of universal machine and universal line models for real-time electromagnetic transient simulation', *IEEE Trans. Ind. Electron.*, 2011, **PP**, (99), p. 1

4 Chen, L., Chen, Y., Xu, Y., Gong, Y.: 'A novel algorithm for parallel electromagnetic transient simulation of power systems with switching events'. Int Conf on Power System Technology (POWERCON) 2010, 2010, pp. 1–7

5 Dufour, C., Mahseredjian, J., Bélanger, J., Naredo, J.L.: 'An advanced real-time electro-magnetic simulator for power systems with a simultaneous state-space nodal solver'. Transmission and Distribution Conf and Exposition: Latin America (T&D-LA), 2010 IEEE/PES, 2010, pp. 349–358

6 Liu, Y.-J., Chang, G.W., Hong, R.-C., Chao, C.-Y.: 'Applications of real-time simulation techniques for shunt active power filter design'. Power & Energy Society General Meeting, 2009. PES'09. IEEE, 2009, pp. 1–5

7 Aguilar, R., Pérez, F., Orduña, E.: 'High-speed transmission line protection using principal component analysis, a deterministic algorithm', *IET Gener. Transm. Distrib.*, 2011, **5**, (7), pp. 712–719

8 Pérez, F.E., Orduña, E., Guidi, G.: 'Adaptive wavelets applied to fault classification on transmission lines', *IET Gener. Transm. Distrib.*, 2011, **5**, (7), pp. 694–702

9 Bo, Z.Q., Jiang, F., Chen, Z., Dong, X.Z., Weller, G., Redfern, M.A.: 'Transient based protection for power transmission systems'. IEEE Power Engineering Society Winter Meeting, 2000, vol. 3, pp. 1832–1837

10 Duan, J., Zhang, B., Luo, S., Zhou, Y.: 'Transient-based ultra-high-speed directional protection using wavelet transforms for EHV transmission lines'. Transmission and Distribution Conf. and Exhibition: Asia and Pacific, 2005, IEEE/PES, pp. 1–6

11 Figueroa, M.A., Orduña, E.: 'Ultra-high-speed protection for medium voltage distribution networks with distributed generation'.

Transmission and Distribution Conf. and Exposition: Latin America, 2008 IEEE/PES, 2008, pp. 1–8
12 Abdel-Rahman, M., Semlyen, A., Iravani, M.R.: 'Two-layer network equivalent for electromagnetic transients', *IEEE Trans. Power Deliv.*, 2003, **18**, (4), pp. 1328–1335
13 Matar, M., Iravani, R.: 'A modified multiport two-layer network equivalent for the analysis of electromagnetic transients', *IEEE Trans. Power Deliv.*, 2010, **25**, (1), pp. 434–441
14 Porkar, B., Vakilian, M., Feuillet, R.: 'Frequency-dependent network equivalent for electromagnetic transient studies by vector fitting'. Proc. Transmission and Distribution Conf. Exhibition, Dallas, TX, May 2006, pp. 166–171
15 Freitas, F.D., Martins, N., Varricchio, S.L., Rommes, J., Veliz, F.C.: 'Reduced-order transfer matrices from RLC network descriptor models of electric power grids', *IEEE Trans. Power Syst.*, 2011, **26**, (4), pp. 1905–1916
16 Kurokawa, S., Prado, A.J., Pissolato, J., Bovolato, L.F., Daltin, R.S.: 'Alternative proposal for modal representation of a non-transposed three-phase transmission line with a vertical symmetry plane', *Latin Am. Trans. IEEE (Revista IEEE America Latina)*, 2009, **7**, (2), pp. 182–189
17 Moreira, F.A., Marti, J.R.: 'Latency techniques for time-domain power system transients simulation', *IEEE Trans. Power Syst.*, 2005, **20**, (1), pp. 246–253
18 Moreira, F.A., Marti, J.R., Zanetta, L.C.: 'Latency techniques applied to the transient simulation of transmission lines using the *Z*-line model'. IEEE Transmission & Distribution Conf. and Exposition: Latin America, 2006. TDC'06, 2006, pp. 1–6
19 Moreira, F.A., Mart, J.R., Zanetta, L.C., Linares, L.R.: 'Multirate simulations with simultaneous-solution using direct integration methods in a partitioned network environment', *IEEE Trans. Circ. Syst. I Regul. Pap.*, 2006, **53**, (12), pp. 2765–2778
20 Semlyen, A., de León, F.: 'Computation of electro-magnetic transients using dual or multiple time steps', *IEEE Trans. Power. Syst.*, 1993, **8**, (3), pp. 1274–1281
21 Zini, H., Rattá, G.: 'Multirate modeling scheme for electromagnetic transient calculation', *IEEE Trans. Power Deliv.*, 2003, **19**, pp. 240–247
22 Burt, P.J., Adelson, E.H.: 'The Laplacian Pyramid as a compact image code', *IEEE Trans. Commun.*, 1983, **Com-3l**, (4), pp. 532–540
23 Vaidyanathan, P.P.: 'Multirate systems, and filter banks' (Prentice Hall P T R, 1993)
24 MATLAB the Language of Technical Computing, software, The MathWorks Inc., R2010
25 Dommel, H.W.: 'Digital computer solution of electromagnetic transients in single and multiphase networks', *IEEE Trans. Power Appar. Syst.*, 1969, **88**, (4), pp. 388–399
26 EMTP Theory Book – Branch of System Engineering Bonneville Power Administration, Portland, Oregon, USA, 1995

9 Appendix

9.1 Models parameters

The following tables summarise the main parameters of the test system and its implemented models (Tables 3–8).

Transfer functions are of the form $(a_0 + a_1z^{-1} + a_2z^{-2} + \cdots + a_nz^{-n}/1 + b_1z^{-1} + b_2z^{-2} + \cdots + b_nz^{-n})$

9.2 Filter coefficients

Coefficients of the FIR filters used in the scheme MMD are obtained by the following commands in Matlab (Fig. 11).

Coefficients of the FIR filters used in the scheme MM1C are obtained by the following commands in Matlab (Fig. 12).

Table 3 Impedances of the test network

	R, Ω	*X*, Ω 50 Hz
*Z*1	5.10	102.04
*Z*2	8.33	2500.00
*Z*3	8.33	2500.00
*Z*4	514.36	1186.10
*Z*5	8.33	2500.00
*Z*6	8.33	2500.00
*Z*7	11.90	238.10
*Z*8	697.34	1247.70
*Z*9	3.97	1190.50
*Z*10	23.81	476.19
*Z*11	605.71	1412.40
*Z*12	397.04	418.95
*Z*13	14.29	285.71
*Z*14	10.42	3125.00
*Z*15	426.95	564.65
*Z*16	71.43	1428.6
*Z*17	532.57	870.11
*C*1, *C*2, *C*3 y *C*4	0	−30.666

Table 4 Coefficients of *A*(*z*) (positive sequence) model MC

Coefficient	*A*(*z*) EMTP scheme				
	Line length, km				
	90	150	180	240	510
*a*0	0.951306036206872	0.919854643395376	0.887486904698236	0.837142613962501	0.645289792469380
*a*1	−2.696032166036320	−2.673917014529040	−2.190554111528240	−2.146165849516750	−1.560872525454590
*a*2	2.698461124927630	2.814903422079430	1.881270401347960	1.905521743366470	1.276655752423030
*a*3	−1.085398569363710	−1.259905395812890	−0.649297552366144	−0.661001037542185	−0.392954818249203
*a*4	0.132276697608974	0.199607063927762	0.073507110180150	0.065862456055184	0.033377685079065
*b*1	−2.855431817352190	−2.937320814551700	−2.523117001057020	−2.652191637637130	−2.654748286116680
*b*2	2.890767327441660	3.134559380520840	2.237535810778190	2.480197555458890	2.505688705828840
*b*3	−1.186267358067850	−1.429083638701890	−0.811778201210917	−0.941688205976846	−0.983722445093812
*b*4	0.151547620305235	0.232391511564330	0.099792827448792	0.115057604305765	0.134313773378965

doi: 10.1049/iet-gtd.2011.0827

Table 5 Coefficients of $A(z)$ (positive sequence) model MMD – low-frequency channel

Coefficient	$A(z)$ MMD scheme – low-frequency model			
	Line length, km			
	150	180	240	510
$a0$	0.966761128266594	0.958087674361397	0.941892271540906	0.873781077779450
$a1$	−1.070438209753390	−0.771687034827360	−0.841181363220360	−0.745852191106656
$a2$	0.258020297319976	0.063768837958935	0.101538701092299	0.080230355782518
$a3$	−0.001083253116142	0.000814051890679	0.001744806228300	0.006534603123853
$a4$	−0.000023816050481	−0.000000364733569	−0.000008533382246	−0.000003794889652
$b1$	−1.125532237648820	−0.829636160260947	−0.928233674332062	−0.936675946689180
$b2$	0.284376334567494	0.082834328445176	0.135461000470601	0.156718668712488
$b3$	−0.004558136313734	−0.000063418443434	−0.000933005170314	−0.000205786935517
$b4$	0.000000459412288	0.000000000097947	0.000000000406587	0.000000001910757

Table 6 Coefficients of $A(z)$ (positive sequence) model MMD – high-frequency channel

Coefficient	$A(z)$ MMD scheme – high-frequency model			
	Line length, km			
	150	180	240	510
$a0$	0.919854643395376	0.887486904698236	0.837142613962501	0.645289792469380
$a1$	−0.466622050465483	−0.326184425413592	−0.259618326941665	−0.141208880083994
$b1$	−0.537118358548963	−0.421638537037902	−0.397442048551721	−0.452150705851506

Table 7 Coefficients of $A(z)$ (positive sequence) model MM1C

Coefficient	$A(z)$ MM1C scheme – low-frequency model			
	Line length, km			
	150	180	240	510
$a0$	0.954342815350193	0.941732654200430	0.918012106226555	0.820506489813600
$a1$	−1.505083667564240	−1.109764642194560	−1.206154058103120	−1.003030461647650
$a2$	0.653642800312933	0.268151522859415	0.372551150562130	0.237130251369857
$a3$	−0.057725869089026	−0.001322315708133	−0.012678244430220	0.022230532642678
$a4$	−0.000112257821050	−0.000085559968868	−0.000544166592689	−0.000544179386105
$b1$	−1.603113963650120	−1.213162437790270	−1.365901800452260	−1.352310617106060
$b2$	0.722221071400487	0.321063470102157	0.468727027073448	0.446034029224241
$b3$	−0.074412220841581	−0.008353051677837	−0.030853006199070	−0.015645484992821
$b4$	0.000677799593240	0.000009896842041	0.000020163997512	0.000043712208702

Table 8 Coefficients of $Zc(z)$ (positive sequence)

Coefficient	$Zc(z)$ for all lines			
	Model MC	Model MMD (low frequency)	Model MMD (high frequency)	Model MM1C
$a0$	226.531778814320000	227.216949477003000	225.822	226.972571465588000
$a1$	−1350.068139858060000	−1194.931517558970000	–	−1266.844160553050000
$a2$	3363.579613061050000	2595.776204406430000	–	2938.591225436240000
$a3$	−4495.083272742080000	−2977.457995292270000	–	−3625.231732925830000
$a4$	3417.288418416750000	1898.770541631430000	–	2507.959958770440000
$a5$	−1423.307005829910000	−636.903108139692000	–	−922.162879257315000
$a6$	271.870169521048000	87.516031851416600	–	140.673650651932000
$a7$	−10.811561383127200	0.012893656873191	–	0.041366412613017
$b1$	−5.961489123325770	−5.262191604477850	–	−5.583639064370460
$b2$	14.858152462167300	11.438954734983500	–	12.957416798343000
$b3$	−19.866660260887500	−13.131110164905500	–	−15.992845214154600
$b4$	15.114902793898500	8.381541788344020	–	11.070427612685000
$b5$	−6.303934584826190	−2.814613910688020	–	−4.073791731879620
$b6$	1.207974260626210	0.387419156868045	–	0.622431880288267
$b7$	−0.048945547652573	−0.000000000000079	–	−0.000000280909199

```
%Antialias Filter (order 76)
a10=firls(76,[0 0.035 0.11 1],[1 1 0 0])

%Interpolator Filter (order 38)
b10=intfilt(10,2,0.1)
```

Fig. 11 *Coefficients of the FIR filters used in the scheme MMD*

```
%Antialias Filter (order 76)
a5=firls(76,[0 0.15 0.2 1],[1 1 0 0])

%Interpolator Filter (order 48)
b5=intfilt(5,5,1/5)
```

Fig. 12 *Coefficients of the FIR filters used in the scheme MM1C*

doi: 10.1049/iet-gtd.2011.0827